Flow Turbulence Combust (2008) 81:97–114
DOI 10.1007/s10494-008-9152-4

Coherent Structures and their Frequency Signature in the Separated Shear Layer on the Sides of a Square Cylinder

C. Brun · S. Aubrun · T. Goossens · Ph. Ravier

Received: 13 February 2007 / Accepted: 7 April 2008 /
Published online: 30 May 2008

Abstract The purpose of the present work is to study the various specific time scales of the turbulent separating flow around a square cylinder, in order to determine the Reynolds number effect on the separating shear layer, where occurs a transition to turbulence. Unsteady analysis based on large eddy simulation (LES) at intermediate Reynolds numbers and laser doppler velocimetry (LDV) measurements at high Reynolds numbers are carried out. The Reynolds number, based on the cylinder diameter D and the inflow velocity U_o, is ranging from $Re = 50$ to $Re = 300{,}000$. A special focus is performed on the coherent structures developing on the sides and in the wake of a square cylinder. For a large Reynolds number range above $Re \approx 1,000$, both signatures of Von Karman (VK) and Kelvin–Helmholtz (KH) type vortical structures are found on velocity time samples. The combination of their frequency signature is studied based on Fourier and wavelet analysis. In the present study, We observe the occurrence of KH pairings in the separating shear layer on the side of the cylinder, and confirm the intermittency nature of such a shear flow. These issues concerning the structure of the near wake shear layer which were addressed for the

C. Brun (✉) · S. Aubrun · T. Goossens
Laboratoire de Mécanique et d'Énergétique, Institut PRISME,
8, rue Léonard de Vinci, 45072 Orléans, France
e-mail: christophe.brun@univ-orleans.fr

T. Goossens
PSA, 78943 Vélizy, France

Ph. Ravier
Laboratoire d'Etude du Signal et de l'Informatique, Institut PRISME,
Site Galilée, 45072 Orléans, France

round cylinder case in a recent experimental publication (Rajagopalan and Antonia, Exp Fluids 38:393–402, 2005) are of interest in the present flow configuration as well.

Keywords Shear layer instability · Kelvin–Helmholtz structures · Near wake · Large-eddy simulation · Laser doppler velocimetry

1 Introduction

The flow over a cylinder is a multiscale problem in the sense that 'the shear layer separating from the edge of the cylinder shares features with mixing layers, flow with recirculation, and separated boundary layers' [20]. As a consequence, hydrodynamic instabilities which develop in the near wake are of at least two types, Kelvin–Helmholtz (KH) like instability in the separated shear layer and Von Kármán (VK) instability in the wake [23]. The interaction between these two features of the flow has been intensively studied with both experimental [16, 23, 31] and numerical [4, 9] approaches since the detailed preliminary work of Bloor [2] who stated that 'Transition to turbulence occurs before the separated layer rolls up in the wake...and is observed at all Reynolds number larger than $Re = 1{,}300$'. She demonstrated that the ratio of the 'transition wave frequency' (presently denoted shear layer frequency f_{SL}) to the 'fundamental frequency' (presently denoted Kármán frequency f_K) was almost proportional to $\sqrt{Re}$. This issue led to a lot of controversy in the last twenty years and was addressed in many papers [9, 16, 23, 24, 29, 31]. In a recent experimental publication by Rajagopalan and Antonia [24], a special attention is given to the shear layer instability characteristics on the sides of a circular cylinder in the Reynolds number range $740 \leq Re \leq 14{,}800$. Mainly, four issues are addressed which concern (1) the critical Reynolds number when the instability first appears at about $Re_c = 1{,}480$, (2) the dependence on the Reynolds number of the ratio between the shear layer frequency and the vortex shedding frequency $f_{SL}/f_V = 0.029\,Re^{0.65}$, (3) the existence of vortex pairing in the separating shear layer that supports the arguments that the near wake flow develops via a convective instability mechanism similar to the one observed in plan mixing layers, (4) the identification of two different flow regimes for $Re \leq 5{,}000$ and $Re \geq 5{,}000$. In the present study which focuses on the near wake flow behind a square cylinder, all these observations are qualitatively confirmed with some small quantitative changes due to the difference in the geometrical configuration. The purpose of the present work is to study the various specific time scales of the turbulent separating flow on the sides of a square cylinder, a configuration which has received much less detailed interest as far as the shear layer feature and the interaction between KH and Kármán vortical structures is concerned [19, 20]. For a large Reynolds number range above $Re \approx 1{,}000$, both signatures of VK and KH type vortical structures are found on velocity time samples. If the VK signature is present at any time in the sample, the KH signature is not. According to previous studies on square and circular cylinder wakes [2, 20, 23, 24], the intermittent generation of KH type vortical structures is due to the unsteady state of the separating shear layer and is phased with the VK instability. One of the objectives of the present study is to determine the Reynolds number effect on the separating shear layer, in the flow regimes where occurs a transition to turbulence.

Unsteady analysis based on both large eddy simulation (LES) at intermediate Reynolds number (Section 2) and laser doppler velocimetry (LDV) measurements at high Reynolds number (Section 3) are presently carried out. The Reynolds number, based on the cylinder diameter D and the inflow velocity U_o, is ranging from $Re = 50$ to $Re = 300{,}000$. We first focus on time-averaged properties of the wake flow (Section 4). Section 5 consists of a qualitative description of the coherent structures developing on the separating shear layer on the sides (KH type vortical structures) and in the wake (VK type vortical structures) of a square cylinder. The intermittent frequency signature related to the combination of KH and VK instabilities in velocity signals makes the use of Fourier transform based signal processing difficult to interpret. In Section 6, a wavelet analysis is performed and compared to the classical Fourier analysis.

2 Numerical Tools

$2D$ direct numerical simulations (DNS) with 87,954 grid points at low Reynolds number $Re \leq 110$ and large eddy simulations (LES) with 693,000 grid points at intermediate Reynolds number $500 \leq Re \leq 2{,}000$ (Table 1) were performed. A parallel version (eight processors when needed) of the Trio_U code developed at the CEA Grenoble was used to solve the incompressible Navier–Stokes equations [14]. The computation domain extends on $L_x = 14D$ in the streamwise direction, $L_y = 13D$ in the transverse direction and $L_z = 4D$ in the spanwise direction, which yields $L_y/D = 7.7\%$ blocage effect for the square cylinder. The discretisation was a staggered finite volume method. Space derivatives were centered fourth order for the convection. A third order Runge–Kutta scheme was used for time advancement. The pressure field was calculated using an SSOR conjugate gradient solver. A local grid refinement was applied close to the cylinder so that no wall treatment was necessary in the transverse y direction. In contrast, a relative low resolution was achieved in the spanwise z direction ($\Delta z = 0.2D$) in comparison with other numerical studies involving DNS for $Re = 500$ with $\Delta z = 0.15D$ [28], $\Delta z = 0.20D$ [26], and LES for $Re = 21{,}400$ with $\Delta z = 0.167D$ [27], $0.08D \leq \Delta z \leq 0.32D$ [25]. The present choice of discretisation is coherent with the objective of the study to accurately determine

Table 1 Mean parameters of the flow simulations

	Re	L_x	L_y	L_z	$n_x \times n_y \times nz$	Cd	Cp_b	St
2D DNS	50–110	$14D$	$13D$	–	$321 \times 274 \times 1$	1.5–1.4	−0.9	$0.133 - 0.171$
DNS [28]	500	$22D$	$18D$	$6D$	$209 \times 129 \times 41$	1.84	−1.24	0.122
DNS [26]	500	$24D$	$10D$	$6D$	$218 \times 104 \times 32$	2.17	–	0.116
LES	500–1,500	$14D$	$13D$	$4D$	$220 \times 175 \times 18$	–	–	$0.12 - 0.14$
LES	1,500	$14D$	$13D$	$8D$	$220 \times 175 \times 37$	–	–	0.133
LES	1,500	$14D$	$13D$	$8D$	$220 \times 175 \times 132$	–	–	–
LES	2,000	$14D$	$13D$	$4D$	$220 \times 175 \times 18$	2.6	−2.0	0.132
LES [25]	21,400	$20D$	$12D$	$4D$	$274 \times 280 \times 50$	2.20	–	0.125
LES [27]	22,000	$22D$	$18D$	$6D$	$185 \times 105 \times 25$	2.03	−1.3	0.126

KH structures which are known to be $2D$ instabilities in the initial stage of their formation [32]. The resulting simulations were therefore well resolved LES in the streamwise and transverse directions, while they were close to VLES in the spanwise direction. Energy spectra for all the three velocity components will be further shown and will confirm the accuracy of the present computations in the spanwise direction in term of energy redistribution. To confirm that the number of resolved modes in the spanwise direction is enough for the present LES study we performed another computation at $Re = 1{,}500$ for a larger domain size $L_z = 8D$ instead of $L_z = 4D$ with the same resolution, which leads to 37 grid points in the spanwise direction (Table 1). We show that the resulting Strouhal number is of the same order of magnitude (Fig. 1) and that the topology of the flow in the separated shear layer on the sides of the cylinder is very similar (Fig. 3b and d). The 3D topology of the flow is out of the scope of the present study. To fully capture such feature, we also performed a highly resolved simulation with 132 grid points in the spanwise direction which yields $\Delta z = 0.05D$ and is presented elsewhere [6] to describe precisely the occurrence of streamwise vortices. Figure 3b, d and f shows that all the three simulations behave qualitatively in the same way concerning the development of the 2D KH instability which is the main scope of the present study.

A selective structure function type SGS model [17] was used. The ratio between eddy-viscosity and molecular viscosity (not shown) is negligible in the near wake while it reaches values larger than 1 in the rear of the cylinder where the VK structures are shedded and advected and the flow yields a fully turbulent state. A constant uniform velocity U_o was imposed as inflow condition. Unlike the case of

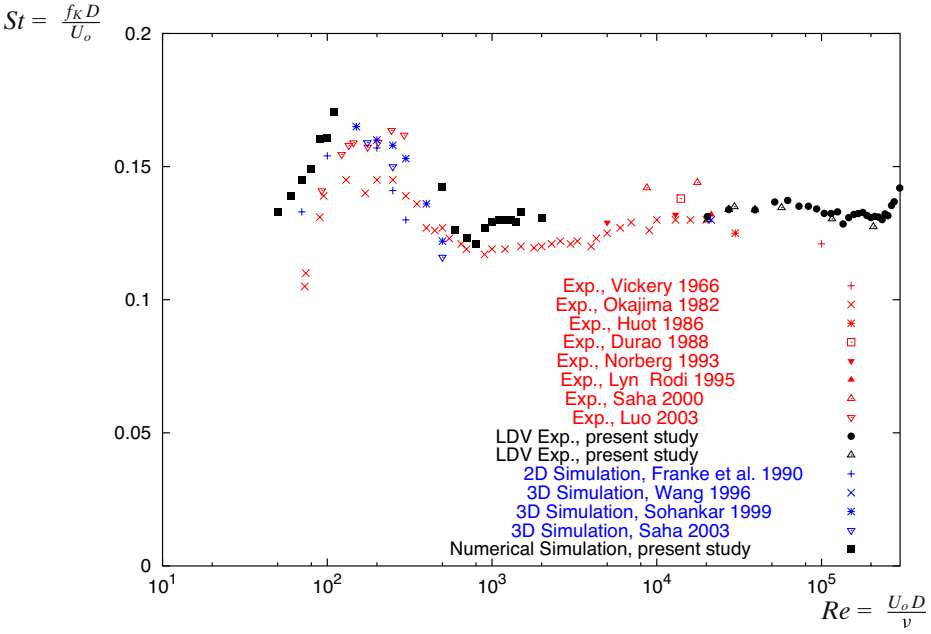

Fig. 1 Strouhal number versus Reynolds number

spatially developing turbulent boundary layers [10] or spatially developing turbulent shear layers [1] where the design of proper realistic turbulent inflow conditions is an issue, no superimposed noise was necessary in the present case. The main reason is that for the considered Reynolds number regime $Re = 500$–$2{,}000$, the boundary layer around the cylinder is laminar above the flow separation and gets turbulent in the separated shear layer downstream in the near-wake [32]. Indeed, the quasiperiodic flow property of the Kármán vortex street which is an hydrodynamic instability of absolute nature is enough to trigger the transition to turbulence which occurs in the separated shear layer.

Outflow advection conditions were applied [22] in the streamwise direction. Free-slip boundary conditions were applied in the transverse and spanwise directions. No-slip velocity boundary condition were set on the cylinder wall.

3 Experimental Facility

Experiments were conducted in a low speed wind tunnel with a $L_y \times L_z = 2 \times 2$ m test section. A square cylinder with a diameter $D = 100$ mm was placed at a distance $x - x_o = 20D$ downstream of the contraction outlet. The size of the test section yields a sufficient aspect ratio L_z/D (Table 2) to obtain a wake development with negligible end effects. At the inlet of the test section, the channel boundary layer was about 1 cm thick. The measured velocity profiles at midspan had less than $\langle U \rangle / U_\infty = 0.5\%$ of spatial non-uniformity and less than $u'/U_\infty = 0.8\%$ of turbulence level. The use of a settling chamber and of a contraction with a ratio 6.25:1 is useful to reduce as much as possible the non-homogeneity and the turbulence level of the inflow velocity field. With this respect, experiments and numerical simulations have relative similar low turbulence inflow conditions.

Non-intrusive velocity measurements were performed using a two components laser doppler velocimetry (LDV) system which consisted of a Dantec bichromatic Argon laser with a size of the measuring volume at the intersection of two laser beams $Lo \times ho \times ho = 1.74$ mm $\times$ 90.5 μm $\times$ 90.5 μm, and a fringe spacing $i =$ 3.74 μm. The flow was seeded with DEHS particles ($C_{26}H_{50}O_4$) of size about $0.2 - 0.3$ μm and low density with a very long life time (4 h) and a high refraction coefficient (about 1.45), which was useful when seeking high frequency samples of about 10 to 20 kHz. Non-intrusive properties of the LDV technique allowed to investigate the full recirculation zone on the sides of the cylinder. The drawback

Table 2 Mean parameters of the flow experiments

	Re	L_x	L_y	L_z	Cd	Cp_b	St
LDV	20, 000	$50D$	$20D$	$20D$	–	–	0.131
LDV	27,000	$50D$	$20D$	$20D$	–	–	0.134
LDV	40,000	$50D$	$20D$	$20D$	–	–	0.134
LDV	50,000–300,000	$50D$	$20D$	$20D$	–	–	0.130–0.140
Visualisations	10,000–170,000	$50D$	$20D$	$11D$	–	–	–
HW [13]	22,000–100,000	$50D$	$20D$	$11D$	2.10	−1.3	0.130–0.135

related to such a technique is that a constant high frequency sampling is only obtained with the condition of data interpolation, but biased errors are reduced when a high frequency sampling is used, which is the present case. Strouhal numbers obtained from LDV measurements compare well with 2D Hot Wire measurements performed elsewhere [12, 13] in the outer recirculation region (Table 2).

In addition, smoke visualisations were performed (Fig. 5). Illumination was provided by a Nd:YAG laser (Spectra Physics 400) to generate images with a resolution of 1,008 × 1,016 pixels, high enough to precisely describe small scale KH vortices at high Reynolds number.

4 Statistical Results

For a square cylinder, the first Hopf bifurcation yields at about $Re = 47 \pm 2$ the formation of the large scale VK street [28]. In the Reynolds number range presently studied, the related vortex shedding frequency is about $St = \frac{f_K D}{U_o} \approx 0.15$ [30]. Williamson [32] and Luo et al. [18] describe the wake behind a round and a square cylinder respectively. For low Reynolds number regime $Re \leq 150$ they observe that the flow is laminar and quasi-periodic with a periodical vortex shedding but without transition to turbulence and no three-dimensionality (without dislocations and streamwise vortices). For this reason it is clear that the spanwise velocity component is identically zero and a 2D numerical computation is enough to describe exactly and without approximation the flow behind a cylinder at low Reynolds number. Thus it makes sense to call such a 2D simulation for $50 \leq Re \leq 110$ a direct numerical simulation of the Navier–Stokes equations. The validation of the numerical code in the present flow configuration was partly performed based on these $2D$ simulations at low Reynolds number. The onset of the VK absolute instability and its Reynolds number dependency $St \times Re = 0.18Re - 3.7$ are well predicted (Fig. 1) [28].

Strong three-dimensional aspects of the flow appear at approximately $Re \geq 150$–200 [28]. The flow separates at the upper corner to form a recirculating zone on the sides of the cylinder. At this regime the separating shear layer remains stable and the transition to turbulence occurs in the far wake. LES performed at $Re = 500$–2,000 are in the range for which the KH instabilities develop in the separated shear layer on the sides of the cylinder. Consequently, RMS velocity profiles reach a maximum value located in the middle of the mean shear zone of the recirculation. For $Re = 2{,}000$, it is clear that transition to turbulence appears in the shear layer between $x = 0.25D$ and $x = 0.5D$ (Fig. 2b, d and f). For increasing Reynolds number, the transition moves further upstream in the shear layer up to $x \leq 0.20D$ as can be seen from LDV measurements for $Re = 20{,}000$ (Fig. 3b, d and f). Mean velocity profiles determined from LES results at $Re = 2{,}000$ and LDV measurements at $Re = 20{,}000$ (Figs. 2a, c, e and 3a, c, e) show the same qualitative trend in term of recirculation zone on the top of the cylinder and fit existing experimental results [20]. Nevertheless, important quantitative changes can be observed when Reynolds number is increased. First, the wall friction distribution is modified. At $x = 0.5D$, it is maximum for $Re = 20{,}000$ while it is nearly zero for $Re = 2{,}000$, a result which can be understood as the effect of the development of a secondary recirculating zone at the wall of the cylinder and which was already observed on PIV measurements [12]. Second, integral quantities

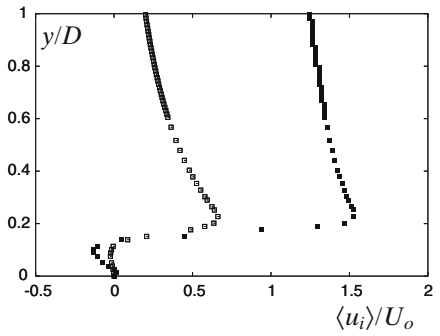

a Mean profiles for $x = 0.20D$.

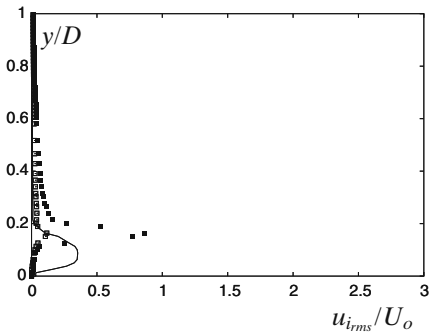

b RMS profiles for $x = 0.20D$.

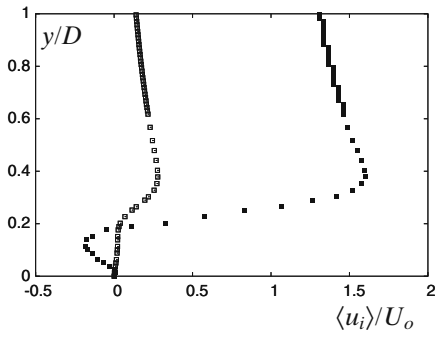

c Mean profiles for $x = 0.50D$.

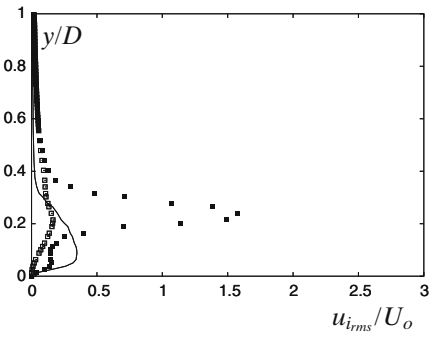

d RMS profiles for $x = 0.50D$.

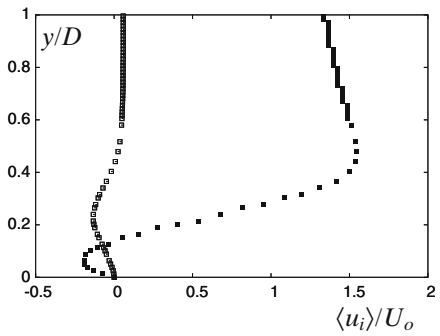

e Mean profiles for $x = 0.80D$.

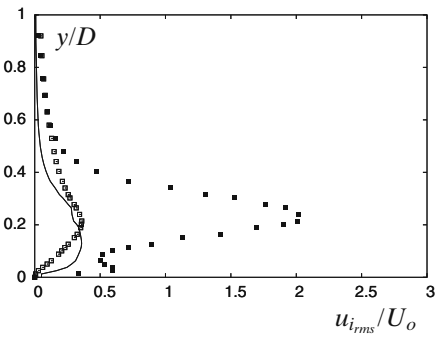

f RMS profiles for $x = 0.80D$.

Fig. 2 Mean and RMS velocity profiles in the separated flow on the sides of a square cylinder from LES computations for $Re = 2{,}000$. *Black square* streamwise velocity u, *square* transverse velocity v, *line* spanwise velocity w

such as vorticity thickness $\delta_\omega = u_{\max}/\frac{\partial u}{\partial y}_{\max}$ and momentum thickness θ_o are Reynolds number dependent, which is consistent with the behaviour of standard mixing layers. They reach respectively $\delta_\omega = 0.062D$ and $\theta_o = 0.0132D$ for $Re = 2{,}000$ at $x = 0.25D$ and $\delta_\omega = 0.0158D = 1.58$ mm and $\theta_o = 0.0047D = 0.47$ mm for $Re = 20{,}000$ at $x = 0.2D$. These results are in the range of the expected values for mixing layers in the sense that δ_ω is about three to five times larger than θ_o.

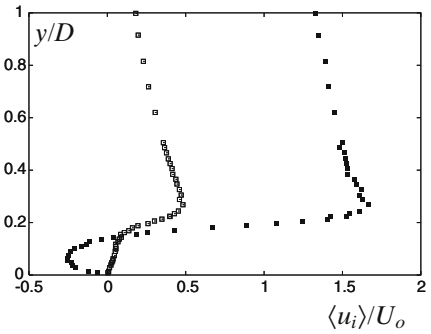

a Mean profiles for $x = 0.30D$.

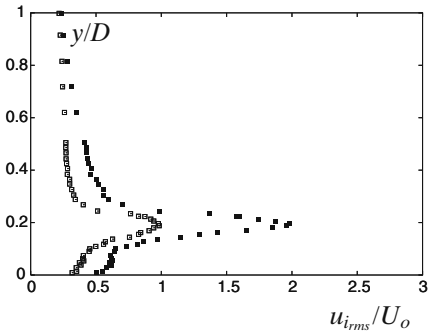

b RMS profiles for $x = 0.30D$.

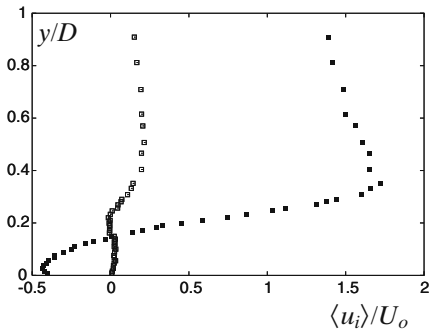

c Mean profiles for $x = 0.60D$.

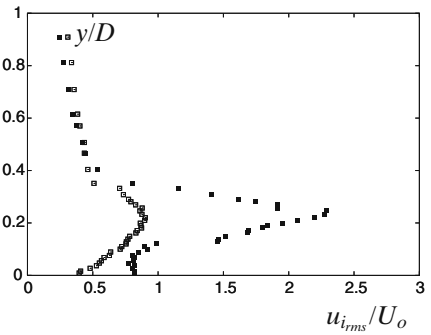

d RMS profiles for $x = 0.60D$.

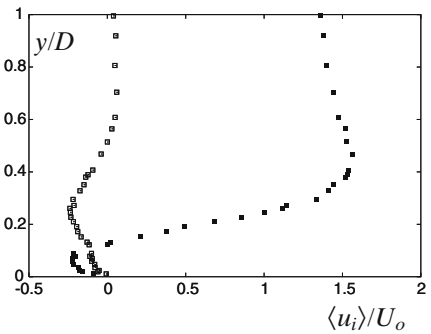

e Mean profiles for $x = 0.90D$.

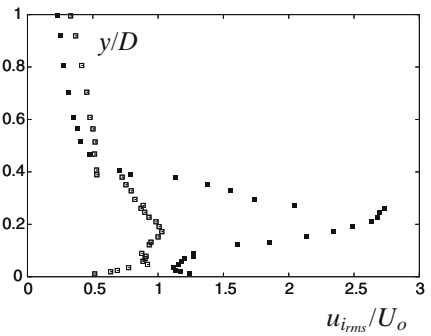

f RMS profiles for $x = 0.90D$.

Fig. 3 Mean and RMS velocity profiles in the separated flow on the sides of a square cylinder from LDV measurements for $Re = 20{,}000$. *Black square* streamwise velocity u, *square*, transverse velocity v

5 Coherent Structure Analysis

Figure 4 shows a slice of the norm of the vorticity on the sides of a square cylinder determined from LES in the range $500 \leq Re \leq 2{,}000$. Shear zones related to the separating shear layer appear in dark grey. For $Re = 500$ the shear layer remains stable and rolls up to form the Kármán vortex street in the rear of the cylinder. For

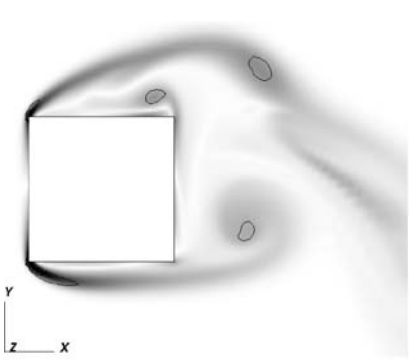

a $Re = 500$ $(L = z = 4D, \Delta_z = 0.2D)$

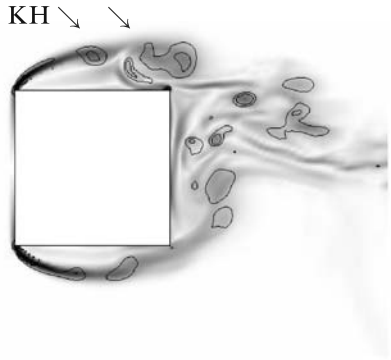

b $Re = 1,500$ $(L = z = 4D, \Delta_z = 0.2D)$

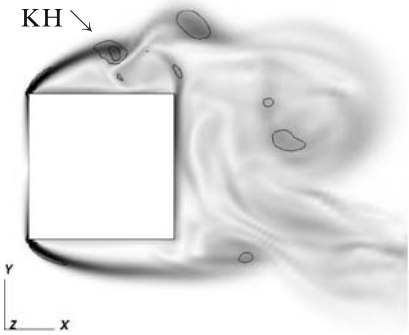

c $Re = 1,000$ $(L = z = 4D, \Delta_z = 0.2D)$

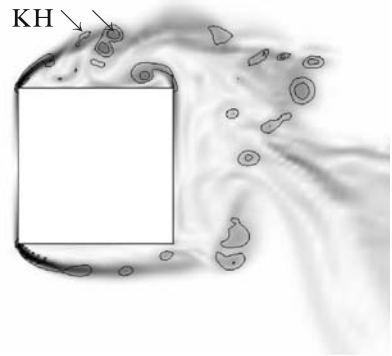

d $Re = 1,500$ $(L = z = 8D, \Delta_z = 0.2D)$

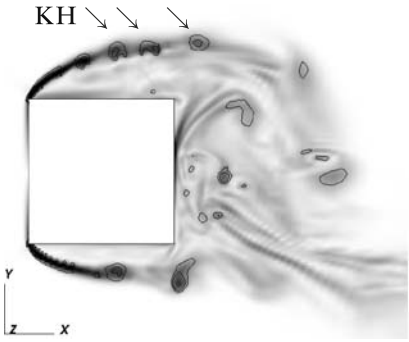

e $Re = 2,000$ $(L = z = 4D, \Delta_z = 0.2D)$

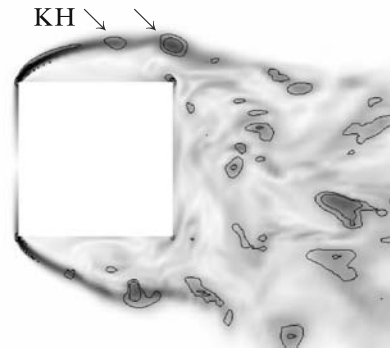

f $Re = 1,500$ $(L = z = 8D, \Delta_z = 0.05D)$

Fig. 4 KH structures developing in the separated shear layer on the sides of a square cylinder, computed with LES in the range $500 \leq Re \leq 2{,}000$ (Table 1). Norm of the vorticity (*grey scale*) and Q-criterion (isolines $Q = 3U_o^2/D^2$, and $Q = 5U_o^2/D^2$)

$Re \geq 1{,}000$ the shear layer gets unstable and KH vortical structures (marked with an arrow on Fig. 3) appear on the sides of the cylinder before to be engulfed in the large scale vortex street in the rear of the cylinder. The onset of the development of KH

instabilities in the separated shear layer on the sides of a square cylinder is similar to the one obtained for a round cylinder about $Re = 1{,}300$ [2, 20]. Isovalues of the Q-criterion plotted on Fig. 4 are useful to count the number of vortical structures in the shear layer. For the present visualisations we observe two KH structures for $Re = 1{,}000$, three KH structures for $Re = 1{,}500$ and four KH structures for $Re = 2{,}000$. Most of those structures are finally pairing before being absorbed in the wake of the cylinder. For higher Reynolds number, smoke visualisations (Fig. 5) show that the number of visible KH structures does not grow but their size clearly decreases and the position of first pairing moves forward to the upper corner of the cylinder. The first KH structure developing in the shear layer is located at about $x = 0.2D$ for $Re = 2{,}000$ (Fig. 4e) and at $x = 0.05D$ for $Re = 22{,}000$ (Fig. 5a). For increasing Reynolds number, transition to turbulence which is associated to a strong turbulent mixing of the smoke moves up to the origin of the shear layer as well. An interesting aspect of the KH phenomenology is their interaction with the recirculating flow along the wall. Figure 4d top and 4f bottom show KH structures located in $x = 0.5D$ which are being convected back to the cylinder corner in the recirculating flow. Those coherent structures are finally absorbed in the separating shear layer to merge with an advected KH structure in a process which might be complex and will be described further in the paper. Note that such behaviour has not been observed at high Reynolds number, the reason being certainly that the transition to turbulence takes place too close to the upper corner of the cylinder to have a chance to interact with possible KH structures advected backward in the recirculating flow.

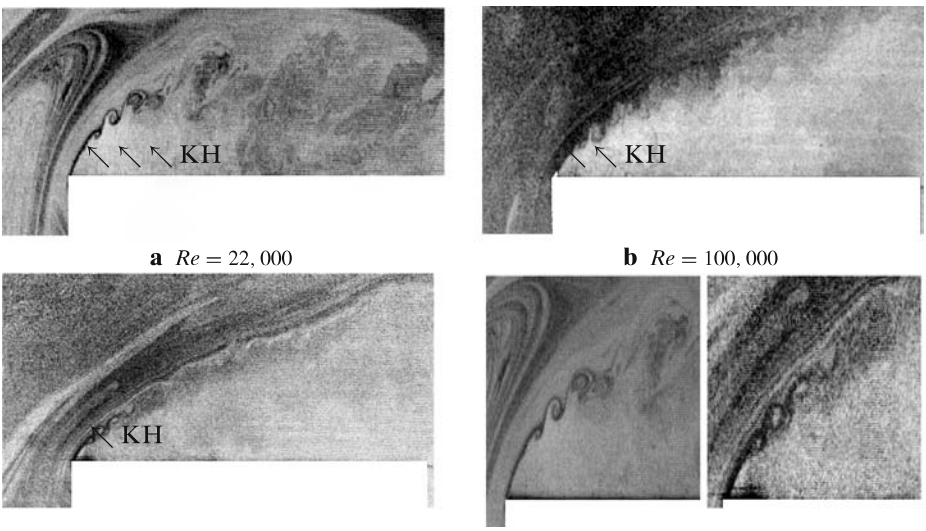

a $Re = 22,000$ **b** $Re = 100,000$

c $Re = 166,000$ **d** zoom: $Re = 22,000$ & $Re = 166,000$

Fig. 5 KH structures developing in the separated shear layer on the top of a square cylinder. Smoke visualisations (extracted from [12])

6 Time-frequency Analysis

Instantaneous velocity time samples are strongly unsteady in the separated shear layer on the sides of the cylinder. The flow is perturbed by large scale motions due to the Kármán vortex street developing in the wake and by the transition to turbulence occurring in the shear layer, characterised by the presence of KH vortical structures. Both contribution act at different time scales and the KH signature appears intermittently on velocity signals. Though VK and KH frequencies are identifiable using Fourier analysis, this method is not well adapted to quantify the energy content of the KH frequency. Indeed, the Fourier transform is not localised in time and the intermittency of the velocity signal leads to a distortion of the spectrum, a drawback which was already observed for the round cylinder case [23]. It results in an underestimation of the actual energy content at this frequency and a spreading over of the energy content to neighbour frequencies. In the present section, results based on both Fourier analysis and wavelet analysis are presented. The latter has the great advantage of supplying a frequency description localised in time. It will help to compare more accurately energy contained in VK and KH signatures [3]. It also can be used to design a specific conditional averaging and quantify the intermittency related to the KH structures [5].

6.1 Fourier analysis

Figures 6 and 7 show the density energy spectra for each velocity component taken in the separated shear layer for $Re = 2{,}000$ (LES) and $Re = 27{,}000$ (LDV), respectively. The signature in spectra of the shear layer instability f_{SL} and of the primary vortex shedding instability f_K is similar to the one intensively studied for a round cylinder configuration [23, 24, 29] and more recently for two side-by-side circular cylinders with a small gap arrangement [7, 15].

For a square cylinder at $Re = 2{,}000$ the frequency f_{SL} is clearly visible on the spectra at the initial stage of the KH formation close to the upper corner of the cylinder. For $Re = 27{,}000$, the high frequency resolution associated with the present LDV measurement procedure allows to precisely quantify f_{SL} as about 40 times larger than the VK frequency f_K [12, 13]. Figures 7c shows the strong Reynolds

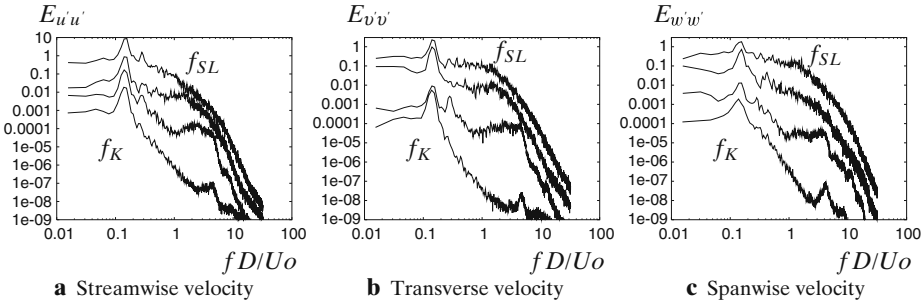

Fig. 6 Frequency analysis of the flow velocity in the separated shear layer on the sides of a square cylinder. Density energy spectra: LES for $Re = 2{,}000$ at ($x = 0.D$, $x = 0.25D$, $x = 0.50D$ and $x = 0.75D$ from *bottom to top*)

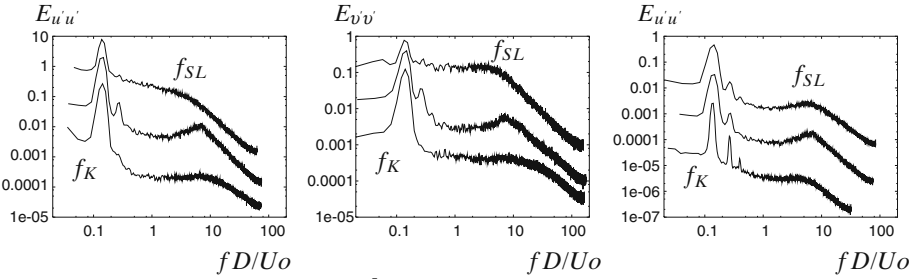

a Streamwise velocity **b** Transverse velocity **c** Reynolds number effect

Fig. 7 Frequency analysis of the flow velocity in the separated shear layer on the sides of a square cylinder. Density energy spectra: LDV for $Re = 27{,}000$ at $x = 0.05D$, $x = 0.10D$, $x = 0.20D$ from *bottom to top* (a,b) and for $Re = 20{,}000$, $Re = 27{,}000$, $Re = 40{,}000$ at $x = 0.10D$ from *bottom to top* (c)

number effect in the present regime. The f_{SL} peak is not yet fully developed for the case at $Re = 20{,}000$, is clearly identified at $Re = 27{,}000$, and finally spread over subharmonics at $Re = 40{,}000$. The specific trend in the present case is that successive pairings between vortices rapidly occur on the sides of the cylinder. It leads to the extension of a plateau on the energy spectrum centered on a frequency about half f_{KH} for all Reynolds number considered. A more precise analysis requires therefore the use of time-frequency procedures such as wavelet transforms.

6.2 1D wavelet decomposition

A $1D$ continuous wavelet decomposition was performed on streamwise (Fig. 8), transverse (Fig. 9) and spanwise velocity samples (Fig. 10) extracted in the shear layer for $Re = 2,000$ (Figs. 8a, 9a, 10a) and $Re = 27{,}000$ (Figs. 8b, 9b). A complex Morlet wavelet

$$\psi_{T_o,\tau}(t) = \frac{1}{\sqrt{\pi T_o}} e^{2i\pi \frac{t-\tau}{T_o}} e^{-\frac{(t-\tau)^2}{T_o^2}} \tag{1}$$

was used to separate the VK and the KH mode contributions [11]. $1D$ wavelet coefficients

$$C_m(T_o, \tau) = \int_0^\infty u_i'(t)\psi^*_{T_o,\tau}(t)dt \tag{2}$$

were computed for each velocity component $u_i' = u_i - \langle u_i \rangle$ and for reduced frequencies $fD/Uo =$ ranging from 0.07 to 10 (LES) or 100 (LDV), including the VK and the KH frequencies to be analysed. The time-frequency evolution of the modulus of $C_m(f, t)$ and the wavelet coefficient energy which corresponds to its average value $\langle C_m \rangle(f)$ over a full sample are shown on Figs. 8, 9 and 10.

For $Re = 2{,}000$, velocity time series show that VK instabilities are present at any time whereas KH instabilities appear intermittently in the signal. This statement is confirmed by the wavelet coefficient which reaches a constant high level at the VK reduced frequency about $f_K = 0.132Uo/D$, while it shows localised peaks at the KH reduced frequency range $fD/Uo = 1 - 10$. It is clear that these peaks do not always appear at the same frequency. The wavelet coefficient energy shows that two

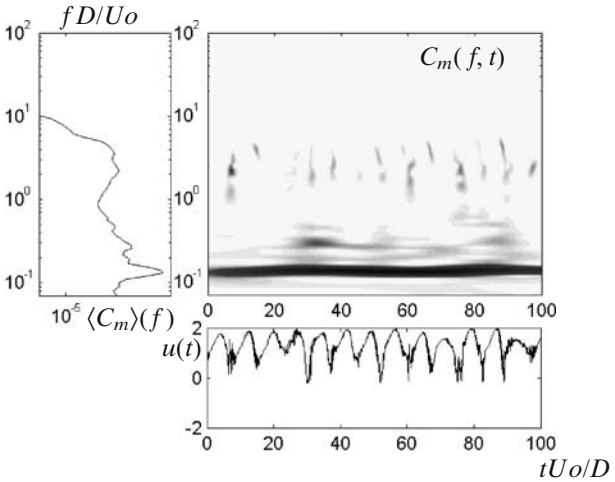

a LES for $Re = 2,000$ streamwise velocity u.
$x = 0.2D$, $y = 0.20D$

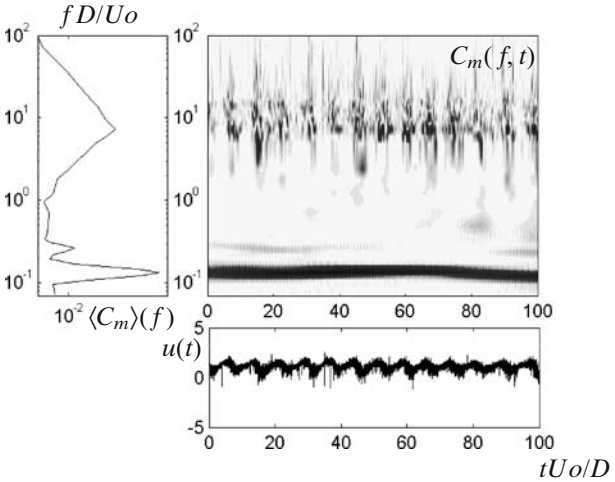

b LDV for $Re = 27,000$ streamwise velocity u.
$x = 0.1D$, $y = 0.105D$

Fig. 8 Time-frequency analysis of the streamwise velocity in the separated shear layer on the sides of a square cylinder. Separation of VK and KH mode contributions based on wavelet transform

reduced frequencies $f_{SL}D/Uo = 2.2$ and 3.5 seem to be dominant. These details were not visible with the Fourier Analysis. The wavelet coefficient energy $\langle Cm\rangle(f)$ shows the same trend as the Fourier analysis, i.e. the KH frequency decreases with increasing longitudinal distance and is progressively overwhelmed in turbulence. For $Re = 27{,}000$, VK instability is still visible on time velocity signals, but small scale turbulence related to transition fill in the high frequency domain. The wavelet coefficient distribution shows very clearly the signature of each instability. The KH instability appears more frequently but it is still focused on two reduced frequencies $f_{SL}D/Uo = 7$ and 14 and the wavelet coefficient magnitude is of the same order for VK and KH frequencies.

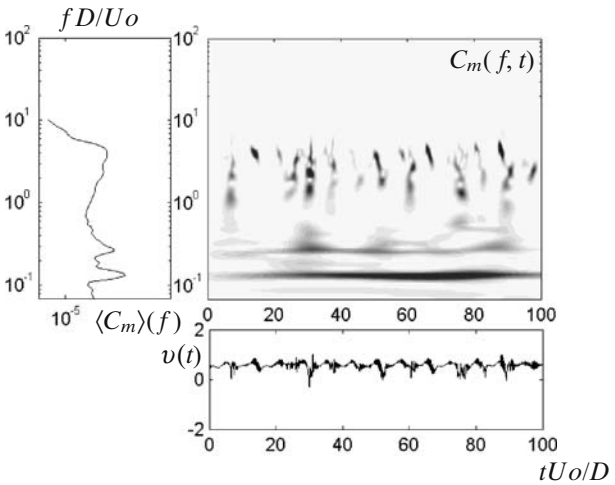

a LES for $Re = 2,000$ transverse velocity υ.
$x = 0.2D$, $y = 0.20D$

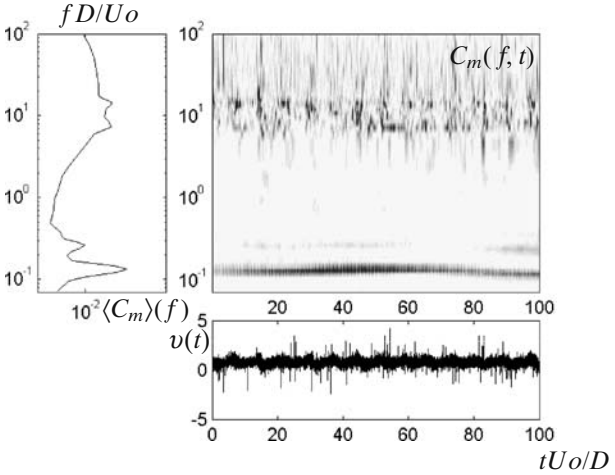

b LDV for $Re = 27,000$ transverse velocity υ.
$x = 0.1D$ $y = 0.105D$

Fig. 9 Time-frequency analysis of the transverse velocity in the separated shear layer on the sides of a square cylinder. Separation of VK and KH mode contributions based on wavelet transform

Linear stability theory applied to mixing layer [21] evaluates the shear layer fundamental frequency at $f_{SL} = 0.033U_c/\theta_o$, based on the momentum thickness and the convection velocity. The present results are roughly in this range for both the intermediate Reynolds number case $f_{SL}\theta_o/U_c \in [0.035, 0.056]$ and the high Reynolds number case $f_{SL}\theta_o/U_c \in [0.013, 0.027]$. The difference with the mixing layer theoretical results seems to be due to the specific configuration which is of the type of a recirculating flow [8]. For such flows the vorticity thickness should be the relevant lengthscale and yield a normalised frequency in the range $f_{SL}\delta_\omega/U_c \in [0.2, 0.3]$. The present results fit completely to these values for both Reynolds number cases: $f_{SL}\theta_\omega/U_c \in [0.18, 0.29]$ and $f_{SL}\theta_\omega/U_c \in [0.15, 0.31]$, respectively. For high Reynolds number, it is relatively obvious that the two frequencies represent the KH

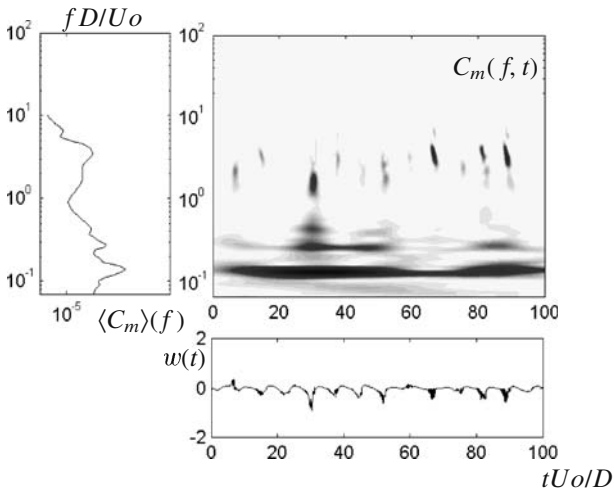

Fig. 10 Time-frequency analysis of the spanwise velocity in the separated shear layer on the sides of a square cylinder. Separation of VK and KH mode contributions based on wavelet transform

LES for $Re = 2,000$ spanwise velocity w.
$x = 0.2D$, $y = 0.20D$

fundamental frequency f_{SL} and its subharmonic $0.5\,f_{SL}$ which result from a pairing mechanism such as shown Fig. 5d. In this case, both the linear stability theory and the recirculating flow analysis perform well. Indeed, at sufficiently high Reynolds number it was observed that the shear layer is rapidly unstable and the transition to turbulence occurs in a localised region close to the upper corner of the cylinder, which yields quasi no interaction with the recirculation region downstream. For the intermediate Reynolds number, the two KH frequencies are not proportional and it is the lower one which corresponds to the linear stability theory. In this case a more complex mixing mechanism seems to play a role, which was observed on Fig. 4d and f where vortical structures are from time to time advected back in the recirculation zone along the wall and are merged with the primary KH vortices. This mechanism, which consists of adding vortical structures characterised by a specific time scale to the classical advected KH structures growing in the shear layer, leads to the formation of higher frequency peaks in the energy spectra which would be harmonics $2\,f_{SL}$ if the backflow velocity was of same magnitude as the advection velocity (which is not the case). This may be the reason why the higher KH frequency determined for $Re = 2,000$ reaches values larger than the fundamental shear layer frequency but different from the second harmonics.

Since the wavelet analysis allows a precise determination of the shear layer fundamental frequency f_{SL}, it is interesting to recast the obtained values with respect to the VK frequency. The ratio f_{SL}/f_K is expected to vary as a power law (close to the square root function [2]) with respect to Reynolds number. A rough computation of this slope based on the two present cases for $Re_1 = 2{,}000$ and $Re_2 = 27{,}000$ yields a value of $n = \frac{ln(f_{SL1}/f_{SL2}) - ln(f_{K1}/f_{K2})}{ln(Re_1/Re_2)} = 0.70$, which fits fully with the existing results for a round cylinder case, $n = 0.67$ [23, 24]. The issue whether a $n = 0.5$ exponent [2, 29] would be in better agreement than the present law would require more analysis based on the present wavelet procedure to separate between fundamental frequency,

Table 3 Fraction of time when the KH instability is visible in transverse velocity signals (intermittency). LES for $Re = 2{,}000$

x/D	Intermittency [%]
0	14.0
0.2	43.9
0.25	45.3
0.5	59.6
0.75	73.5
0.8	58.0

harmonics and subharmonics which must be considered separately in such Reynolds scaling study [9]. This will be performed in future work.

The wavelet coefficient can be used as well as a threshold to perform conditional analysis on the KH instability. It is observed that peak occurrences of $C_m(f,t)$ are phased with the VK instability. The width of each peak is determined using an arbitrary threshold and the fraction of time when the KH instability is present can be deduced as a definition of intermittency coefficient. Table 3 represents the wavelet intermittency coefficient versus the longitudinal position in the shear layer for $Re = 2{,}000$. As expected the intermittency increases with the longitudinal position up to saturation. It illustrates the development of the transition process along the separated shear layer.

7 Conclusions

Extensive data were supplied in the present study concerning numerical and experimental results on the near-wake behind a square cylinder for a large Reynolds number range. A special care was taken during experiments to obtain very high sampling frequency in order to capture properly the high frequency range related to the KH instabilities. The use of the wavelet decomposition allowed a better description of the frequency range involved in KH instabilities and also, gave a tool to perform conditional signal analysis. The present study showed how to quantify the KH instability intermittency using this tool. This method should be improved and extended to other configurations. It would be of special interest in the analysis of the near wake behind a round cylinder which involves a complex relation between KH and VK structures and still yields a relative controversy concerning the intermittency property of the KH instability [24]. For the present square cylinder configuration, it seems that the ratio f_{SL}/f_K is not independent from the Reynolds number and that it follows a similar law as for a round cylinder [23]. Two issues are being addressed as a result of the present analysis. First, the occurrence of pairing [24] is confirmed for the wake behind a square cylinder as well and an accurate tool to determine the fundamental KH frequency is proposed based on wavelet transform. Second, the separation between two regimes for the shear layer instability [24, 29], one at intermediate Reynolds number, another at high Reynolds number is confirmed and a possible relation to the interaction between recirculation at the wall and coherent structures shedding in the shear layer is argued, which was described as breakdown in a recent paper [24].

Acknowledgements The computations were performed on the french national computer center IDRIS with the Trio_U code developed at the CEA Grenoble. The study was part of a DFG-CNRS research project UR 507, untitled 'LES of complex flows'.

References

1. Balarac, G., Métais, O., Lesieur, M.: Mixing enhancement of coaxial jets through inflow forcing: a numerical study. Phys. Fluids **19**, 1–17 (2007)
2. Bloor, M.S.: The transition to turbulence in the wake of a circular cylinder. J. Fluid Mech. **19**, 290 (1964)
3. Bonnet, J.P., Delville, J.: Review of coherent structures in turbulent free shear flows and their possible influence on computational methods. Flow Turbul. Combust. **66**, 333–353 (2001)
4. Braza, M., Chassaing, P., Ha Minh, H.: Numerical study and physical analysis of the pressure and velocity fields in the near wake of a circular cylinder. J. Fluid Mech. **165**, 79 (1986)
5. Brede, M.: Measurement of turbulence production in the cylinder separated shear-layer using event-triggered laser-doppler anemometry. Exp. Fluids **36**, 860–866 (2004)
6. Brun, C., Goossens, T.: 3d coherent vortices in the turbulent near wake of a square cylinder. Comptes Rendus Mécanique **336**(4), 363–369 (2008)
7. Brun, C., Tenchine, D., Hopfiner, E.J.: Role of the shear layer instability in the near wake behavior of two side-by-side circular cylinders. Exp. Fluids **36**(2), 334–343 (2004)
8. Cherry, N.J., Hillier, R., Latour, M.E.M.P.: Unsteady measurements in a separated and reattaching flow. J. Fluid Mech. **144**, 13–46 (1984)
9. Dong, S., Karniadakis, G.E., Ekmecki, A., Rockwell, D.: A combined direct numerical simulation-particle image velocimetry study of the turbulent near wake. J. Fluid Mech. **569**, 185–207 (2006)
10. Ducros, F., Comte, P., Lesieur, M.: Large-eddy simulation of transition to turbulence in a boundary layer developing spatially over a flat plate. J. Fluid Mech. **326**, 1–36 (1996)
11. Farge, M.: Wavelet transform and their applications to turbulence. Annu. Rev. Fluid. Mech. **24**, 395–457 (1992)
12. Goossens, T.: Etude expérimentale et numérique du sillage turbulent et des forces instationnaires sur un obstacle bi-dimensionnel non profilé. In: Ph.D thesis, Université d'Orléans (2005)
13. Goossens, T., Brun, C., Doris, L., Hureau, J.: Kelvin–Helmholtz structures in the separated shear layer on the top of a square cylinder: experimental and numerical investigation. In: ETC 11, Trondheim (2004)
14. Howard, R.J.A., Pourquie, M.: Large eddy simulation of an Ahmed reference model. J. Turbul. **3**(1), 12 (2002) Institute of Physics Pub Ltd.
15. Kim, H.J., Durbin, P.A.: Investigation of the flow between a pair of circular cylinders in the flopping regime. J. Fluid Mech. **196**, 431 (1988)
16. Kourta, A., Boisson, H.C., Chassaing, P., Ha Minh, H.: Non-linear interaction and the transition to turbulence in the wake of a circular cylinder. J. Fluid Mech. **181**, 141 (1987)
17. Lesieur, M., Métais, O.: New trends in large-eddy simulations of turbulence. An. Rev. Fluid. Mech. **28**, 45–82 (1996)
18. Luo, S.C., Chew, Y.T., Ng, Y.T.: Characteristics of square cylinder wake transition fows. Phys. Fluids **17**, 1–4 (2003)
19. Lyn, D.A., Einav, S., Rodi, W., Park, J.-H.: A laser-doppler velocimetry study of ensemble-averaged characteristics of the turbulent near wake of a square cylinder. J. Fluid Mech. **304**, 285–319 (1995)
20. Lyn, D.A., Rodi, W.: The flapping shear layer formed by flow separation from the forward of a square cylinder. J. fluid Mech. **267**, 353–376 (1994)
21. Michalke, A.: On spatially growing disturbances in an inviscid shear layer. J. Fluid Mech. **23**(3), 521–544 (1965)
22. Orlansky, I.: A simple boundary condition for unbounded hyperbolic flows. J. Comp. Phys. **21**, 251 (1976)
23. Prasad, A., Williamson, C.H.K.: The instability of the shear layer separating from a bluff body. J. Fluid Mech. **333**, 375 (1997)
24. Rajagopalan, S., Antonia, R.A.: Flow around a circular cylinder—structure of the near wake shear layer. Exp. Fluids **38**, 393–402 (2005)

25. Rodi, W., Ferziger, J.H., Breuer, M., Pourqui, M.: Status of large eddy simulation: results of a workshop. ASME J. Fluid Eng. **119**(2), 248–262 (1997)
26. Saha, A.K., Biswas, G., Muralidar, K.: Three-dimensional study of flow past a square cylinder at low reynolds numbers. Int. J. Heat Fluid Flow **24**, 54–66 (2003)
27. Sohankar, A., Davidson, L., Norberg, C.: Large eddy simulation on flow past a square cylinder: comparison of different subgridscale models. J. Fluid Eng. **122**, 39–47 (2000)
28. Sohankar, A., Norberg, C., Davidson, L.: Simulation of three-dimensional flow around a square cylinder at moderate reynolds numbers. Phys. Fluids **11**, 288–306 (1999)
29. Thompson, M.C., Hourigan, K.: The shear-layer instability of a circular cylinder wake. Phys. Fluids **17**, 1–4 (2005)
30. Vickery, B.J.: Fluctuating lift and drag on a long cylinder of square cross-section in a smooth and in a turbulent stream. J. fluid Mech. **25**, 481–494 (1966)
31. Wei, T., Smith, C.R.: Secondary vortices in the wake of circular cylinders. J. Fluid Mech. **169**, 513 (1986)
32. Williamson, C.H.K.: Vortex dynamics in the cylinder wake. Annu. Rev. Fluid. Mech. **28**, 477 (1996)